Reviews in Mineralogy & Geochemistry
Vol. 58, pp. 239-257, 2005

$^{40}Ar/^{39}Ar$ Thermochronology of Detrital Minerals

K.V. Hodges*, K.W. Ruhl, C.W. Wobus, M.S. Pringle
Department of Earth, Atmospheric, and Planetary Sciences
Massachusetts Institute of Technology
Cambridge, Massachusetts, 02139, U.S.A.
**kvhodges@mit.edu*

INTRODUCTION

Clastic sediments and sedimentary rocks provide important records of the erosional history of active and ancient orogenic systems. For example, foreland basin deposits are especially rich sources of information about the character of orogenic hinterlands that have long-since eroded away. A popular approach to extracting such information is the U-Pb dating of detrital zircon (e.g., Ross and Bowring 1990; Gehrels 2000); by matching detrital zircon age populations with age patterns in exposed bedrock regions, it is possible to constrain the source regions for basin fill—provided, of course, that what is left of the hinterland is at least representative of what was there at the time of exhumation! One reason that zircon is used for such studies is that it has a very high closure temperature for Pb diffusion, higher that metamorphic temperatures in all but high-temperature granulite settings (Cherniak and Watson 2000), so that detrital U-Pb zircon dates almost always reflect provenance ages. Unfortunately, the refractory nature of the U-Pb zircon system means that it is less useful for understanding the thermal and erosional evolution of the hinterland than other systems with lower closure temperatures. Other chapters in this volume deal with the application of low-temperature (U-Th)/He and fission-track thermochronometers to detrital samples. Here we review the methodology of detrital $^{40}Ar/^{39}Ar$ thermochronology and explore how it has been used in a variety of tectonic studies. Additional perspectives are available in Stuart (2002). We presume a basic familiarity with the fundamentals of $^{40}Ar/^{39}Ar$ geochronology and the laser $^{40}Ar/^{39}Ar$ microprobe; readers who would like a review should consult Harrison and Zeitler (2005) of this volume, McDougall and Harrison (1998), and Hodges (1998).

MOTIVATIONS FOR DETRITAL $^{40}Ar/^{39}Ar$ STUDIES

With the development of laser microanalytical protocols for terrestrial $^{40}Ar/^{39}Ar$ geochronology in the late 1970's and early 1980's, a new dimension was added to studies of detrital minerals. As is the case with the U-Pb zircon method, the $^{40}Ar/^{39}Ar$ method can be used to pinpoint the provenance of detrital minerals. However, it also can be used to establish the cooling histories of source terrains, to constrain the timescales of sedimentary processes, and—in some cases—to define the positions of deformational features that control patterns of uplift in active orogens. While detrital fission-track and (U-Th)/He) thermochronology also offer such insights, the current state of these arts is such that the $^{40}Ar/^{39}Ar$ laser microprobe technique provides considerably higher precision and more rapid sample throughput.

A relatively recent innovation has been the application of detrital $^{40}Ar/^{39}Ar$ thermochronology to modern fluvial sediments. One important motivation for this application is reconnaissance mapping of bedrock cooling ages in modern surface exposures. In active orogenic settings, the method provides a simple and effective way to development regional

1529-6466/05/0058-0009$05.00 DOI: 10.2138/rmg.2005.58.9

maps—catchment by catchment—of exhumation patterns indicative of tectonic evolution. Moreover, when bedrock patterns of cooling ages are known, the technique can be used to explore erosional processes for individual fluvial systems and thus track the geomorphic evolution of mountainous landscapes.

SAMPLING AND SAMPLE PREPARATION

As is the case in other geochemical studies, the sampling of fresh, unaltered materials is important for $^{40}Ar/^{39}Ar$ detrital thermochronology. The best sedimentary rock samples are impure sandstones and arkoses that show no evidence of post-depositional metamorphism. Similarly, the best modern sediments are those with high concentrations of K-rich minerals. In all cases, minerals should be free of obvious signs of alteration. Examining potential samples with a hand lens before collecting them can substantially improve the probability of successful laboratory work. Do K-feldspar grains show signs of authigenic overgrowths that may complicate data interpretation? Are the micas clean, or do they show intergrowths with other minerals that may yield poor $^{40}Ar/^{39}Ar$ results? In some cases, simple ancillary studies—such as the use of illite crystallinity to evaluate the degree of post-depositional metamorphism—can be useful in selecting optimal samples.

Most detrital $^{40}Ar/^{39}Ar$ studies have focused on one mineral, usually either K-feldspar, a dioctahedral mica such as muscovite or phengite, or a trioctahedral mica such as biotite or phlogopite. All are resistant to abrasion and chemical dissolution during transport, and should persist for long distances downstream from the source region (Kowalewski and Rimstidt 2003). K-feldspar yields dates corresponding to the low-temperature evolution of source terrains and thus is especially useful for comparisons with results obtained from detrital zircon fission-track studies (Bernet and Garver 2005). However, feldspars are also very susceptible to alteration, particularly in submarine environments, and most grains derived from metamorphic or intrusive igneous rocks are sufficiently structurally complex that they do not have a single, narrow range of $^{40}Ar/^{39}Ar$ closure temperatures (Parsons et al. 1999; Lovera et al. 2002). Since laser fusion is the most frequently used procedure for $^{40}Ar/^{39}Ar$ detrital geochronology (see below), such complexities can greatly hinder the robust interpretation of K-feldspar data. As a consequence, the majority of modern detrital studies focus on the micas.

Micas are common in clastic sediments, and it is relatively easy to make high-purity separates of them. Because they are elastic at surface conditions, they survive sedimentary transport over long downstream distances with relatively minor grain size reduction. It is possible in some cases to distinguish multiple components within a sample's population of micas on the basis of grain size alone. These may represent different source regions, or different lithologies in the same region. If the provenance cooled very slowly (<1 °C/m.y.), multiple grain size fractions may provide important information about its thermal history due to the grain size dependence of closure temperature (e.g., Markley et al. 2002).

Of the micas, muscovite has proven to be the best mineral for detrital $^{40}Ar/^{39}Ar$ work. The trioctahedral micas can be problematic for several reasons. First, they are highly susceptible to secondary alteration (Mitchell et al. 1988; Dong et al. 1998; Murphy et al. 1998). Small-scale intergrowths of chlorite are common in biotites, and their presence renders a grain unsuitable for $^{40}Ar/^{39}Ar$ dating (Roberts et al. 2001; Di Vincenzo et al. 2003). Second, many biotites contain excess ^{40}Ar not produced by *in situ* decay of ^{40}K and, as a consequence, yield geologically meaningless $^{40}Ar/^{39}Ar$ dates (Kelley 2002). In contrast, dioctahedral micas are less susceptible to alteration and, with the exception of phengite (e.g., Scaillet 1996), only infrequently incorporate excess ^{40}Ar during growth.

Grains can be separated from sands or sedimentary rock samples using a variety of standard mechanical, gravimetric, and magnetic techniques. Because it is desirable to maintain original grain sizes, the best separation protocols involve only as much mechanical crushing as is absolutely necessary. In order to ensure maximum purity, some laboratories leach samples in dilute acids to remove contaminant primary minerals and alteration products. Inevitably, hand picking of individual, optically pure grains is necessary for good analytical results. Most laboratories sieve each sample to two or more grain size ranges. These ranges are analyzed independently in order to test for grain size-dependent, apparent age variations.

Although the sample itself dictates the range of grain sizes available for analysis, the best grain sizes for $^{40}Ar/^{39}Ar$ detrital thermochronology range from approximately 250 to 1000 μm. Substantially smaller grains are difficult to manipulate and, after irradiation, pose significant laboratory safety issues. Moreover, small grains that are very young may not contain sufficient radiogenic ^{40}Ar for a high-precision $^{40}Ar/^{39}Ar$ analysis. Very small grains (<20 μm) may lose ^{39}Ar through recoil during irradiation and yield spurious results (Hunecke and Smith 1976; Onstott et al. 1995; Lin et al. 2000), although methods have been suggested to overcome this limitation (e.g., Hemming et al. 2002).

The number of analyses necessary for a robust result

For all detrital geochronology studies—whether they are based on the $^{40}Ar/^{39}Ar$ method or other techniques—a persistent question is: how many analyses are necessary to characterize adequately the cooling age signal for a particular sample? A typical sedimentary sample is a mechanical mixture of thousands of grains of a datable mineral from an unknown number of source regions. Given that it is practically impossible to date all the grains in such a sample, how many must we date to ensure that we do not miss one or more components altogether? To some extent the answer depends on how many components there are in the sample; if the population is unimodal, a small number of analyses is sufficient. Additionally, the answer depends on the relative proportions of each component; if a sample contains 5000 datable grains but only one is derived from a specific source, all 5000 grains must be dated if we are to be absolutely sure that we do not miss that single component. Unfortunately, we know neither the number of components in a sample nor their relative abundances *a priori*.

In a recent innovative paper, Vermeesch (2004) developed a general statistical relationship among the number of analyzed grains, the fraction of the population represented by the least well-represented component, and the probability that no component was missed in the study. For example, in order to be ~95% confident of not missing a component making up at least 5% of the population, we would have to analyze *at least* 117 grains. Note that this analysis presumes the worst-case scenario: a uniform distribution of components in the sample, all of the same size. Populations with a smaller number of components require fewer analyses to characterize adequately (Ruhl and Hodges 2005), but a good rule of thumb is to analyze 100 or more grains from each sample whenever a sufficient number of optically pure grains is available.

ANALYTICAL TECHNIQUES

Detrital $^{40}Ar/^{39}Ar$ studies are typically done with Ar-ion or CO_2 laser microprobes (Hodges 1998). Ar-ion lasers emit light at a variety of wavelengths, but most is within the blue-green visible spectrum at 514 or 488 nm. CO_2 instruments produce far-infrared light at 10.6 μm, and their lower cost (as compared to Ar-ion lasers) has promoted their widespread use over the past decade. Both blue-green and far-infrared light are readily absorbed by detrital feldspars and micas, and the two microprobes are equally suitable for laser fusion dating of detrital materials. Most Ar-ion or CO_2 laser microprobe systems are fully automated, and enough single-grain analyses to characterize a detrital sample can be done in approximately 48 hours.

Typical gas extractions involve complete fusion of a grain using a defocused laser beam. In some cases, grains are heated incrementally by varying the power output of the laser upward through a series of steps. While time consuming, this approach can help evaluate the possibility of alteration in suspect samples (Najman et al. 2002). In many laboratories, samples suspected of having slight alteration are routinely heated prior to analysis by either: 1) a bakeout of the sample chamber for several hours at low temperatures (e.g., 350 °C); or 2) exposing each grain to the laser set at low power (to achieve a temperature of ~500–600 °C) for a few minutes prior to fusion.

A small number of detrital $^{40}Ar/^{39}Ar$ studies have been done using a focused Nd-YAG laser (1064 nm) to melt 50–100 micron holes in large single crystals (e.g., Kelley and Bluck 1989). More recently, Sherlock et al. (2002) and Haines et al. (2004) have demonstrated the utility of high spatial-resolution mapping of intracrystalline apparent age domains in single detrital micas using an ultraviolet (frequency-quadrupled Nd-YAG) laser microprobe.

Regardless of the laser employed, modern microprobe systems are capable of producing $^{40}Ar/^{39}Ar$ for single, 250–1000 μm grains with a precision of from 0.5 to 1 Ma for smaller crystals and of 200,000 to 500,000 years for larger crystals. (In this paper, all explicit precisions are cited at the 2σ, or ~95% confidence, level.) Some samples that are more fine-grained or contain components of Plio-Pleistocene age yield single-crystal dates of much poorer precision. One solution to this problem is to analyze multigrain aliquots, rather than single grains. However, this approach precludes detailed analysis of the modality of ages because multiple components may be mixed in each aliquot, so it should be used only when single-crystal analyses are impractical.

Data presentation and interpretation

Specific analytical protocols vary from laboratory to laboratory, so it is imperative that papers with detrital $^{40}Ar/^{39}Ar$ data contain a section describing the methods used in some detail. At the very least, the reported information should include: 1) the name of the reactor used for sample irradiations (because different reactors have different neutron flux and thermal characteristics); 2) the duration of irradiation and the specific position in the reactor; 3) the specific values used to correct for interfering nuclear reactions during irradiation; 4) the name and assumed age of the material used as a neutron fluence monitor; 5) isotopic discrimination factors for the mass spectrometer used for the analyses; and 6) a description of the analytical backgrounds or "blanks" during the measurements. Detailed discussions of these parameters may be found in McDougall and Harrison (1998).

Typically, reported uncertainties for $^{40}Ar/^{39}Ar$ dates represent analytical imprecision at the 2σ (or ~ 95% confidence) level. When uncertainties in the age of neutron flux monitors and uncertainties in ^{40}K decay constants are also propagated into the error as well, the quoted uncertainty reflects the accuracy of the measured date (Renne et al. 1998). However, as is the case with all geochronologic data, a $^{40}Ar/^{39}Ar$ date for a detrital mineral grain is not necessarily a geologically meaningful age. For example, alteration may yield dates that are too young, and ^{39}Ar recoil loss may result in dates for very small grains that are too old. Both problems can be avoided by careful sample selection and the use of appropriate experimental protocols. A grain may be contaminated by excess ^{40}Ar and the laser fusion technique may not provide evidence of that contamination. In some of these cases, laser incremental heating of a representative number of grains may help eliminate this possibility or demonstrate the unreliability of some dates (e.g., White et al. 2002). Another complication can be the existence of significant intracrystalline gradients in radiogenic ^{40}Ar related to slow cooling (Hodges and Bowring 1995) or polymetamorphism (Hames and Hodges 1993). For samples containing older grains, this possibility can be assessed by reconnaissance use of ultraviolet laser microprobes to map individual crystals (Sherlock et al. 2002).

Once the possibility of such "geologic error" has been dismissed, most detrital $^{40}Ar/^{39}Ar$ data interpretation is based on analytical imprecision alone. This statistical measure is useful for exploring the range of apparent ages in a sample population irradiated in a single package and analyzed in a single laboratory using the consistent protocols. The frequency distribution of detrital mineral ages in a sample is typically depicted using either histograms or graphs of the synoptic probability density function (SPDF). The familiar histogram is adequate for small datasets with an age dispersion much greater than the uncertainty of individual analyses, but it is far less valuable for data exploration than a graph of the SPDF. Derived from the probability density functions for individual measurements with known uncertainties*, the SPDF is a normalized summation of such functions for each measurement in a population. Assuming that analytical precision follows a Gaussian distribution, the SPDF for a population of n dates can be written as:

$$SPDF = \frac{\sum_{i=1}^{n}\left(\frac{1}{\sigma_i\sqrt{2\pi}}\right)e^{-(t-t_i)^2/2\sigma_i^2}}{n} \quad (1)$$

where t is age, t_i is the i^{th} measured age, and σ_i is the standard deviation of the i^{th} age†. Sircombe (2004) recently presented a useful discussion of the relative merits of SPDF graphs and histograms, and he has made available for download a Microsoft Excel spreadsheet for producing both from a user-supplied dataset. For example, Figure 1 is a combined histogram and SPDF plot generated with this software for a set of 111 detrital muscovite $^{40}Ar/^{39}Ar$ dates for sands from the Nyadi River in central Nepal (Ruhl and Hodges 2005).

Inferring population characteristics

The Nyadi River has a relatively small drainage area (~200 km^2), so it comes as no surprise that the SPDF in Figure 1 displays a single mode or "hump"—the detrital micas have a range of $^{40}Ar/^{39}Ar$ dates that reflects the unroofing history of the bedrock in the catchment rather than multiple source regions with significantly different unroofing histories. Figure 2 illustrates a very different distribution of $^{40}Ar/^{39}Ar$ muscovite dates. Analyses from several samples of the Triassic part of the Torlesse Supergroup of New Zealand (Adams and Kelley 1998) reveal a decidedly multimodal SPDF. The two groups of apparent ages comprise ranges from ~150–300 Ma and from ~400–500 Ma, suggesting two different source regions. For the purposes of Adams and Kelley (1998), this distinction was sufficient to draw an important tectonic conclusion regarding the source area for *most* of the detrital muscovites: of all the candidate sources, only the New England and Hodgkinson fold belts of northern New South Wales and eastern Queensland, Australia, have the appropriate range of bedrock cooling ages. But what if there was not such a marked age distinction between the modes, or what if there was a value in developing a quantitative understanding of the distinctive modes that might be present? A more sophisticated statistical approach is needed to address such issues.

One of the most widely used methods of modal analysis is mixture modeling (Galbraith and Green 1990; Sambridge and Compston 1994). After the user specifies a number of assumed components, the modeling routines set about finding the best-fit modes, their uncertainties, and relative proportions. For the Torlesse data shown in Figure 2, a search for two components using the Sambridge and Compston approach results in the definition of components at 448 ± 49 Ma and 235 ± 18 Ma. Clearly, these two components alone cannot explain the total dispersion in the dataset, particularly the large number of apparent ages younger than 225 Ma

* For a review of the underlying statistics, see Bevington and Robinson (1992).

† For ease of reference, variables used throughout this chapter are defined in Table 1.

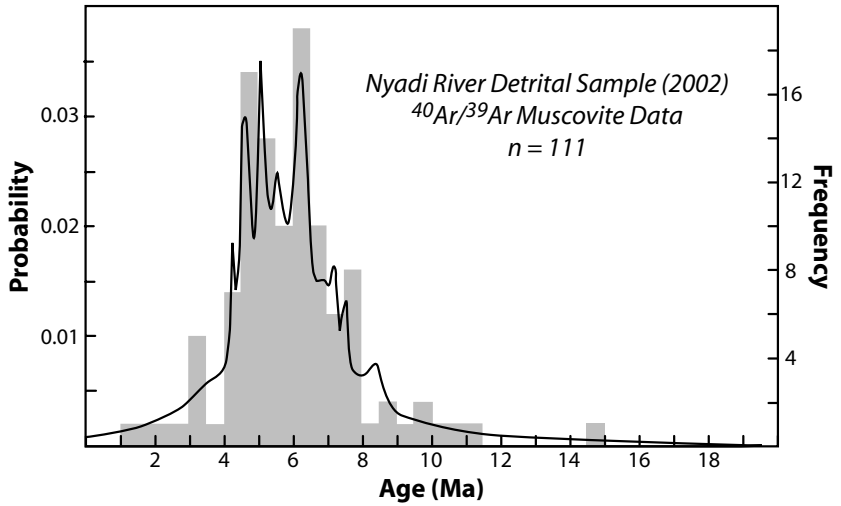

Figure 1. Combined histogram and synoptic probability density function (SPDF) plot for 111 single-crystal, total-fusion, muscovite dates from a modern sand sample collected in 2002 from the Nyadi River, Annapurna Range, central Nepal (Ruhl and Hodges 2005). The histogram (gray boxes) was constructed using a bin size of 500,000 years. A sample collected from the same river bed in 1997 yielded a statistically indistinguishable SPDF plot for 34 multigrain analyses of detrital muscovites (Brewer et al. 2001), implying that there is little year-to-year variability in the age distribution of muscovites in well-mixed sediment samples from this river.

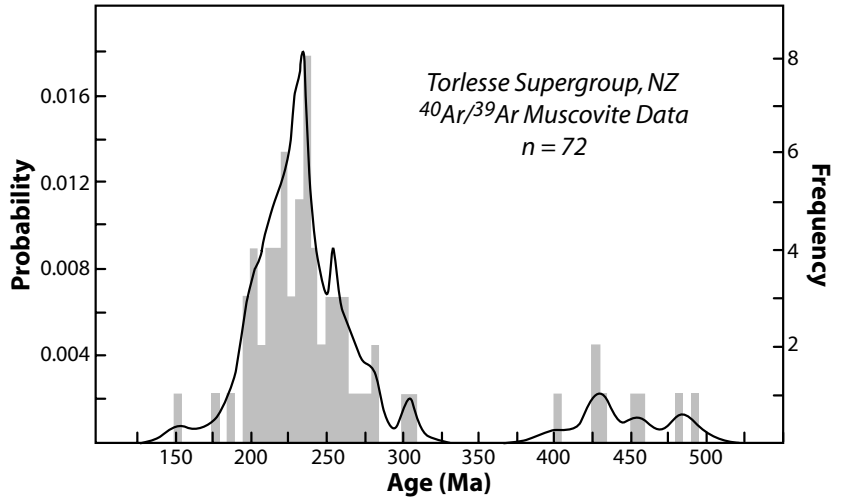

Figure 2. Combined histogram and SPDF plot for 72 $^{40}Ar/^{39}Ar$ muscovite dates from samples of the Triassic Torlesse Supergroup from New Zealand (Adams and Kelley 1998). The bin size for the histogram is 5 million years. Although the age distribution forms two broad groupings (400–500 Ma and 150–300 Ma), at least eight distinct modes are indicated in the dataset by mixture modeling implying numerous source regions with distinctive cooling ages.

Table 1. Symbols used.

Symbol	*Definition*
A_s	Surface volumetric heat production
C	Specific heat
$CSPDF$	Cumulative probability distribution function
E	Erosion rate
G_o	Nominal geothermal gradient (e.g., 25 °C/km)
h	Depth at which heat production drops off to 1/e of A_s
L	Lag time
L_o	Lag time for a mineral in the oldest studied horizon of a sedimentary section
n	Number of measured cooling ages in a series
R	Relief in a stream catchment
$SPDF$	Synoptic probability density function
t	Age
t_m	Measured cooling age
T_m	Bulk closure temperature for an isotopic chronometer
T_{mi}	Cooling age measurement i in a series of n = 1 to i measurements
t_{range}	Range of cooling ages in a distribution
T_s	Surface temperature
T_λ	Assumed temperature at depth λ (e.g., 750 °C)
z	Depth
z_m	Depth of the bulk closure isotherm for an isotopic chronometer
$\Delta\tau_E$	Time elapsed between cooling of a mineral through Tc_m and its exposure at the surface as a consequence of erosion
$\Delta\tau_{TR}$	Time elapsed between initial surface exposure of a detrital mineral and its sedimentary deposition
κ	Thermal diffusivity
λ	Assumed layer thickness for thermal model (e.g., 30 km)
ρ	density
σ_i	Sample standard deviation of the i^{th} measured cooling age in a series of n measurements

and between ~250 and ~300 Ma. Sambridge and Compston (1994) suggest specifying successively larger numbers of modes for analysis until the modeling results stabilize (e.g., the same mode is picked more than once, or the uncertainties in the modes do not decrease as the number of specified modes increase). The Torlesse dataset is very complicated in this regard. The apparent ages in the older group are sufficiently few that the ~448 Ma mode, while robust, is hard to refine further. Mixture modeling experiments with the younger group define robust modes at ~290 Ma, ~233 Ma, ~210 Ma, and ~170 Ma, but a mixture of at least eight modes would be necessarily to describe the full complexity of the data.

This relatively objective approach to analyzing mixed populations provides a powerful tool for comparative studies of detrital age datasets. For example, Gehrels (2000) and Gehrels et al. (2002) showed how the similarities and distinctions between two distributions of U-Pb

detrital zircon data could be quantified. Sircombe and Hazelton (2004) have presented a more sophisticated statistical protocol for testing the similarity of modes in different samples.

APPLICATIONS AND EXAMPLES

In the paragraphs that follow, we examine how $^{40}Ar/^{39}Ar$ geochronology of modern and ancient detrital minerals may be used to address important problems in tectonics and geomorphology.

Determining sediment source regions

The Adams and Kelley (1998) study reviewed above is an example of one of the most common uses of detrital mineral dating: establishing provenance. Among the $^{40}Ar/^{39}Ar$ community, this approach was pioneered by Kelley and Bluck (1989; 1992) in their studies of detrital micas from the Ordovician Southern Uplands sequence of Scotland. Subsequent research demonstrated the applicability of the technique to understanding sedimentary transport in a variety of continental settings (e.g., Renne et al. 1990; Dallmeyer et al. 1997; Stuart et al. 2001; Barbieri et al. 2003; Rahman and Faupl 2003; Haines et al. 2004). In some studies, the fingerprinting of source regions has helped inform large-scale, tectonic reconstructions (e.g., Dallmeyer and Neubauer 1994; von Eynatten et al. 1996; Hutson et al. 1998; Carrapa et al. 2004a) . Changes in provenance with time, as evidenced by variations in cooling age SPDFs from one stratigraphic level to another, have helped to constrain the evolution of drainage patterns (e.g., Aalto et al. 1998; Najman et al. 2003; von Eynatten and Wijbrans 2003; Carrapa et al. 2004b) and the deformational histories of source regions (e.g., White et al. 2002). Although there have been few $^{40}Ar/^{39}Ar$ dating studies of fine-grained terrigenous sediments in oceanic environments, Hemming et al. (2000; 2002) reported impressive results for hornblendes and micas from ice-rafted detritus in Quaternary North Atlantic sediment cores that indicate derivation from the Labrador Sea region.

Constraining minimum depositional ages of ancient sediments

In some cases, sedimentary successions contain abundant detrital minerals suitable for $^{40}Ar/^{39}Ar$ dating but no fossils or volcanogenic strata providing an indication of the age of deposition. Najman et al. (1997) demonstrated how the cooling ages for detrital minerals provide at least a minimum estimate of the depositional age. More recently, Carrapa et al. (2004a) showed how such indirect dating has helped to constrain tectonic models for the Alps-Apennine junction area.

Estimating the timing of source region exhumation

The geochronology of detrital minerals is a powerful way to explore the exhumation histories of orogenic hinterlands. Copeland and Harrison (1990) used $^{40}Ar/^{39}Ar$ data from Ocean Drilling Program sediment cores in the distal Bengal Fan to demonstrate that rocks metamorphosed during the Himalayan orogeny had been uplifted to the surface and were providing detritus to the fan by Middle Miocene time. More detailed investigations of the timing of Himalayan rock uplift have involved dating detrital K-feldspar and micas from more proximal foreland deposits (Harrison et al. 1993; Najman et al. 1997; Najman et al. 2001; Najman et al. 2002). Other case studies of this type include those of Grimmer et al. (2003), who sought to determine the timing of exhumation of ultrahigh-pressure rocks of the Dabie Shan orogen, and Barbieri et al. (2003), who documented the episodicity of uplift in the Ligurian Alps.

Constraining the erosion-transport interval for orogenic detritus

The interval between the cooling age of a detrital mineral and the depositional age of the sedimentary rock in which it is found is frequently referred to as “lag time” (Cerveny et al.

1988; Brandon and Vance 1992; Ruiz et al. 2004). Lag time (L) can be expressed as:

$$L = \Delta\tau_E + \Delta\tau_{TR} \tag{2}$$

where $\Delta\tau_E$ is the time necessary for sufficient erosion to have occurred to bring the mineral to the surface from the position of its closure isotherm at depth, and $\Delta\tau_{TR}$ is the time necessary for transport of the eroded grain through the fluvial system to its final point of deposition.

In a few cases, L is extremely long, suggesting protracted sediment storage and reworking prior to final deposition (Sherlock 2001). However, many studies suggest that transport intervals can be very brief in river networks draining active orogenic systems (e.g., Copeland and Harrison 1990; Heller et al. 1992). This suggests a mechanism by which L might be used to formulate a rough estimate of erosion rate in the source region. If we specify the closure temperature for a mineral (T_m), and calculate the depth of its closure isotherm (z_m) below Earth's surface using a modeled geothermal gradient, then erosion rate (E) is:

$$E = \frac{z_m}{\Delta\tau_E} = \frac{z_m}{\left(L - \Delta\tau_{TR}\right)} \tag{3}$$

As $\Delta\tau_{TR}$ approaches zero, L approaches $\Delta\tau_E$ and $E \approx z_m/L$. (Note that this rate is averaged over the exhumation interval $\Delta\tau_E$. If that interval is sufficiently long, the averaged rate may not be particularly useful for addressing many tectonic problems.)

An estimate of E made with Equation (3) is only as good as the model used for the geothermal gradient. One approach has been to assume a linear, conductive geotherm (Copeland and Harrison 1990; Renne et al. 1990). For example, an estimated geotherm of 30 °C/km implies that z_m is ~12.2 km for a nominal $^{40}Ar/^{39}Ar$ muscovite bulk closure temperature of 366 °C (Hodges 2003). This approach provides a useful rough estimate of E for regions undergoing slow (<1 km/m.y.) erosional exhumation, but a more widely applicable model must account for advective heat transport. Numerical experiments suggest that well-developed orogenic systems (i.e., those in which the orogenic wedge grows rapidly through accretionary processes) achieve thermal steady states relatively quickly (e.g., Huerta et al. 1998). As a consequence, a first attempt at improving upon Equation (3) might be made simply by adopting a sufficiently sophisticated model for the steady-state geotherm that incorporates both conduction and advection.

By way of example, we might presume that the problem is one-dimensional , involving the vertical conduction of heat as well as the vertical advection of both heat and rock as a consequence of erosion. Moreover, we might postulate an exponential decrease in radiogenic heat production with depth, such that the surface heat production (A_s) falls off to a value of 1/e at depth h. As shown by Manktelow and Grasemann (1997), among others, this situation can be modeled as the thermal structure in a layer of thickness λ with a fixed temperature at depth λ (T_λ). For our purposes, the values we choose for λ and T_λ are not particularly critical as long as λ is substantially greater than z_m. The "steady-state" solution for T_m as a function of z_m is:

$$T_m = T_s + \beta\left[1 - \exp\left(-\frac{z_m}{h}\right)\right] + \gamma\left[1 - \exp\left(-\frac{Ez_m}{\kappa}\right)\right] \tag{4}$$

where

$$\beta = \frac{A_s h^2}{\rho C(\kappa - Eh)} \tag{5}$$

and

$$\gamma = \frac{(T_\lambda - T_s) - \beta\left[1 - \exp\left(-\frac{\lambda}{h}\right)\right]}{1 - \exp\left(-\frac{E\lambda}{\kappa}\right)} \tag{6}$$

If we assume zero sediment transport time ($E \approx z_m/L$), we can modify Equation (6) to relate lag time to source-region erosion rate:

$$T_m \approx T_s + \beta\left[1 - \exp\left(-\frac{EL}{h}\right)\right] + \gamma\left[1 - \exp\left(-\frac{E^2 L}{\kappa}\right)\right] \tag{7}$$

Technically, this is *not* actually a steady-state solution; as erosion progresses, heat producing elements are stripped from the top of the column such that A_s in Equation (5) is time-dependent. Manktelow and Grasemann (1997) suggest how this can be dealt with in an iterative fashion, but ignoring this effect has little impact on our particular application of the model.

Equation (7) could be improved upon still further by taking account of the influence of topography on the form of steady state, near-surface isotherms (Stüwe et al. 1994; Mancktelow and Grasemann 1997). However, this effect is damped with increasing depth and has little effect on the $^{40}Ar/^{39}Ar$ muscovite closure isotherm except when exhumation rates are extremely high (>3 km/my; Brewer et al. 2003). A matter of greater concern is the inability of a one-dimensional model to capture lateral advection of both heat and rock during orogenesis (Ehlers and Farley 2003), and developing more realistic models relating lag time to erosion rate is a topic of on-going research.

Provided that the sediment source region does not change, the comparison of lag times from different stratigraphic levels can be used to monitor changes in source-region cooling rate through time (Ruiz et al. 2004). If there was little variation in the thermal structure of the source region, such changes imply changes in erosion rate. Figure 3 illustrates the implications of variations in L with respect to the lag time of the oldest horizon for which

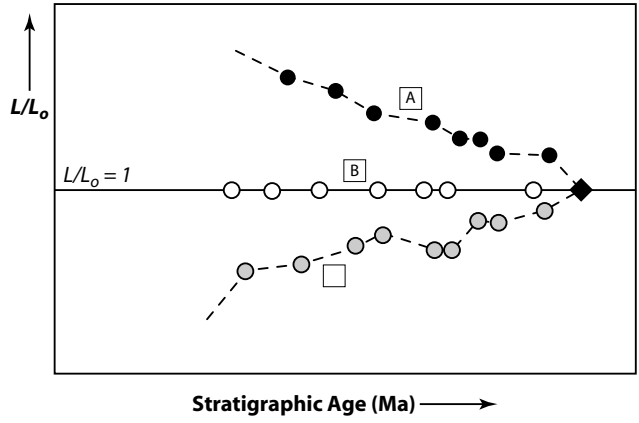

Figure 3. Lag-time evolution diagram. Lag time here is non-dimensionalized by dividing the lag time for a detrital mineral from a horizon of known stratigraphic age (L) by the lag time for that mineral in the oldest studied horizon (L_o). That oldest sample is shown as a filled diamond symbol. Circles indicate lag times for successively younger samples. Curve A implies values of $L/L_o > 1$, implying decreasing source-region erosion rate with time. Curve B ($L/L_o = 1$) suggests a steady state, whereas Curve C ($L/L_o < 1$) suggests an increasing erosion rate with time.

there are thermochronologic data (L_o). Constant lag time at all stratigraphic levels ($L/L_o = 1$) indicates a thermal stability in the source region that suggests steady-state erosion. Equation 3 predicts that increasing cooling rates over time would lead to decreasing lag times ($L/L_o < 1$), and that decreasing cooling rates would have the opposite effect ($L/L_o > 1$). With examples from the Himalaya and Western Alps, White et al. (2002), Carrapa et al. (2003) and Najman et al. (2003) showed how comparative studies of lag times from different stratigraphic levels in foreland deposits can help inform tectonic models for orogenic hinterlands.

Most lag time studies have focused on the lag time between the youngest dated grain in a sample and the sample's depositional age. However, a sample containing multimodal mixtures of grains from multiple source regions contains additional information. If the lag times for two different modes are consistently different through time, the implication is that both eroded at similarly different rates. A convergence of lag times suggests instead a change in the erosional character in one or the other source regions, the minimum age of which can be estimated from the cooling age for the youngest mode at the time of the change (Ruiz et al. 2004).

Elucidating modern erosional patterns

Cooling ages for detrital minerals from modern river networks are powerful indicators of the dynamics of erosion in active orogenic systems. The bedloads of river systems that drain vast continental regions are particularly interesting targets of study; their cooling age spectra provide a sense of large-scale variations in unroofing rate as a consequence of regional tectonic processes. One recent investigation of this type was that of Clift et al. (2004), who combined zircon U-Pb, biotite and muscovite $^{40}Ar/^{39}Ar$, and apatite fission track geochronology to explore the source regions for detritus in the lower Indus River of Pakistan. Their data suggest that the high-grade metamorphic rocks exposed in the physiographic Higher Himalaya are the dominant source of modern sediment. A relatively small proportion of detritus comes from the Nanga Parbat syntaxis, despite evidence for remarkably rapid erosion of that region today (Zeitler et al. 2001).

Estimating erosion rates for modern sedimentary catchments

On a more local scale, thermochronologic data from modern river sediments can serve as a valuable proxy for bedrock cooling ages. Consider a simple landscape, with relatively low topographic relief, that erodes very slowly, no more than one or two millimeters each year (Fig. 4). If this landscape is at least several million years old, chances are that conditions of thermal and topographic steady-state may have been achieved or at least closely approached (Whipple 2001; Willett and Brandon 2002). If we furthermore assume that the only material flux from depth to the surface is related to erosion—such that lateral movements related to tectonic activity are ignored—the $^{40}Ar/^{39}Ar$ cooling ages of minerals exposed on the surface of the landscape will show an elevation dependence; samples from the tops of ridges will yield the oldest dates, and those from the bottoms of valleys will yield the youngest dates. This apparent age gradient with respect to elevation (dt_m/dz) is frequently presumed to be a rough proxy for inverse of the time-averaged erosion rate (E) in regional thermochronologic studies (e.g., Wagner and Reimer 1972). As pointed out by Stock and Montgomery (1996), uniform erosion of such a terrain would yield sediments containing minerals with a range of $^{40}Ar/^{39}Ar$ cooling ages (t_{range}) that is related to the total relief (R) through the equation:

$$t_{range} = R\left(\frac{dt_m}{dz}\right) \tag{8}$$

Stock and Montgomery (1996) suggested how this relationship could be used to explore the evolution of relief in the source regions for modern and ancient sediments if the apparent age gradient with respect to elevation in the bedrock is known.

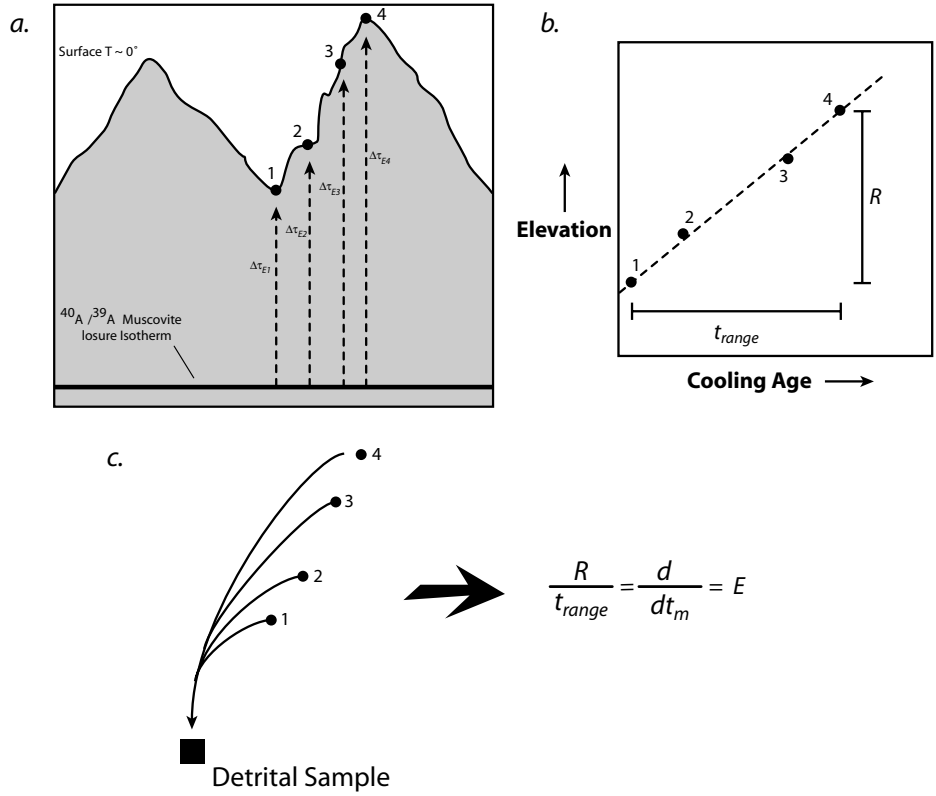

Figure 4. Illustration of how the range of $^{40}Ar/^{39}Ar$ cooling ages for a set of four detrital muscovite samples can be used to estimate source-region erosion rate. (a) Cartoon showing the positions of a range of samples exposed at various elevations in an eroding source terrain. Sample 1 is from the deepest part of the valley and Sample 4 is from the top of the highest ridge. If transport of material from the $^{40}Ar/^{39}Ar$ muscovite isotherm is along vertical paths (shown by dashed lines), Sample 4 should yield the oldest age, having taken τ_{E4} million years to reach the surface, whereas Sample 1 should be the youngest, having taken τ_{E1} million years. The total relief is R and the total range of ages is t_{range}. (b) If Samples 1-4 were collected from bedrock and dated, their $^{40}Ar/^{39}Ar$ cooling ages might be expected to yield a linear relationship with elevation, the slope of which is often interpreted as erosion rate (E). If erosion rate was constant throughout the erosional interval, then E is also equal to R/t_{range}. (c) After muscovite from these samples is eroded and deposited in a river sediment, the range of detrital cooling ages can be used to estimate E *if* we assume that the modern relief of the catchment is the same as the relief during the cooling interval.

For the study of modern catchments with known relief, Equation (2) suggests that the cooling age range also can be used to determine the time-averaged rate of bedrock erosion in the catchment if $E = (dt_m/dz)^{-1}$ (*cf.*, Eqn. 3). An example calculation can be done using the detrital muscovite dataset illustrated in Figure 1 (Ruhl and Hodges 2005), which represents a 13.4 million year range of apparent ages. The total relief in the Nyadi catchment—as measured from a 90-m digital elevation model—is ~6.2 km. As a consequence, we can estimate E as ~0.5 mm/y, although this estimate has large uncertainties related to the high analytical imprecision of very young, single-grain dates in this dataset. If only high-quality dates are used, the apparent age range decreases to ~8.3 million years and the estimate for E increases to 0.75 mm/yr for the period represented by the span of apparent ages (~10.8–2.5 Ma). Note that this rate is only an average. The Nyadi data also imply that the rate of exhumation

increased through the ~10.8–2.5 Ma interval because the young end of the range implies a closure-to-surface transport interval ($\Delta\tau_E$ = 2.5 Ma) that would require erosion rates of several millimeters per year for any reasonable geothermal gradient.

There are two reasons why this simple way of interpreting the data may lead to erroneous results. The first is that developing orogenic systems have complex and time-variant thermal structures, surface topographies, and patterns of material transport (e.g., Batt and Braun 1997; Braun and Sambridge 1997; Stüwe and Hintermüller 2000; Lague et al. 2003) and are not well-represented by the simple model depicted in Figure 4. The second is that erosion rates may vary substantially over a sediment source region, even in small catchments; Safran (2003) presented a useful analysis of how such issues can influence erosion rate estimates.

Fortunately, there are ways to test some of the critical hypotheses implicit in the method described above. If uniform, steady-state erosion is assumed, the *form* of the cumulative probability distribution function (CSPDF) for a set of detrital cooling ages:

$$CSPDF = \sum_{j=0}^{i} SPDF(j) \tag{9}$$

should be the same as the form of the integral hypsometric curve for the catchment (Ruhl and Hodges 2005). If a statistically based comparison of the integral hypsometric and CSPDF curves suggests a poor match, one or more of the assumptions behind using the detrital age range to estimate erosion rate is unjustified. In the case of the Nyadi Khola data, the two curves match very well, lending additional credence to the 0.75 mm/yr estimate for average erosion rate in the catchment over the closure period.

An alternative approach to estimating erosion rates for active river drainage basins was suggested by Brewer et al. (2003).These authors began with a two-dimensional thermal model to estimate the location of the closure isotherm for Ar retention in muscovite beneath a paleosurface as a function of erosion rate and relief. That result can be used to create a "synthetic" SPDF curve for a specified hypsometry, and different synthetic curves can be generated for different assumed erosion rates. Brewer and co-workers suggested that the positions of major peaks in the modeled SPDF curves could be matched with SPDF curves for actual thermochronologic data to find a best-fit erosion rate. However, when this method is applied to a set of detrital muscovite $^{40}Ar/^{39}Ar$ data from the Nyadi catchment (Brewer et al. 2005), it results in an estimated erosion rate of 2.3 mm/yr, almost three times higher than the Ruhl and Hodges (2005) estimate and inconsistent with the observed range of ages (~8.2 million years) over 6.2 km of relief. One likely explanation for this result is that success of the Brewer et al. (2003) approach depends strongly on the fidelity of the thermal model, which itself depends on parameters (e.g., the distribution of radioactive heat producing elements) that are not well constrained for this region of the Himalaya. Moreover, as mentioned previously, lateral advection of both rocks and heat strongly influence the thermal structure of active orogens. Several research groups are currently developing more realistic models that integrate thermal, mechanical, and erosional processes to achieve a more generally applicable method for deducing exhumation rate from the range of detrital mineral ages in modern sediment samples.

Defining the positions of young deformational features

In some cases, the differences in t_{range} for sediments from modern catchments are large enough to allow the definitions of patterns of differential bedrock uplift that are related to deformational features. For example, Wobus and others (2003) used detrital muscovite $^{40}Ar/^{39}Ar$ dating from the Burhi Gandaki and Trisuli river drainages in central Nepal to define better the nature of the steep, roughly E-W-trending topographic transition from the high Himalayan ranges to their southern foothills to the south. Near the transition, small tributaries

enter the major rivers at high angles in a trellised pattern. As a consequence, several of the tributary catchments drain regions north of the transition, whereas others drain regions south of the transition.

Figure 5 shows the SPDF curves for detrital muscovite $^{40}Ar/^{39}Ar$ dates from modern stream sediments collected from these catchments. The curves are markedly different on either side of the transition: almost all grains from tributaries to the north give Miocene or younger apparent ages, while grains from tributaries to the south give Paleozoic or Proterozoic apparent ages. The detrital thermochronologic data suggest that the physiographic transition marks the position of a recently active, south-vergent thrust fault that accommodates uplift of the high Himalayan ranges relative to their foothills. This interpretation gains additional support from cosmogenic ^{10}Be data for sands from the tributary catchments; millennial-timescale erosion rates calculated from those data are four times higher north of the physiographic transition than south of it (Wobus et al. 2005). Although exposures are poor along the transition in the Burhi Gandaki and Trisuli drainages, mapping to the west along strike demonstrates the existence of a system of Pliocene-Quaternary thrust faults with the necessary kinematics to explain the detrital thermochronologic data (Hodges et al. 2004).

FUTURE DIRECTIONS

Detrital mineral $^{40}Ar/^{39}Ar$ thermochronology offers a straightforward, powerful way to explore the tectonic and erosional evolution of orogenic systems and the fluvial networks that transport sediments through them. Because the nominal closure temperatures of $^{40}Ar/^{39}Ar$

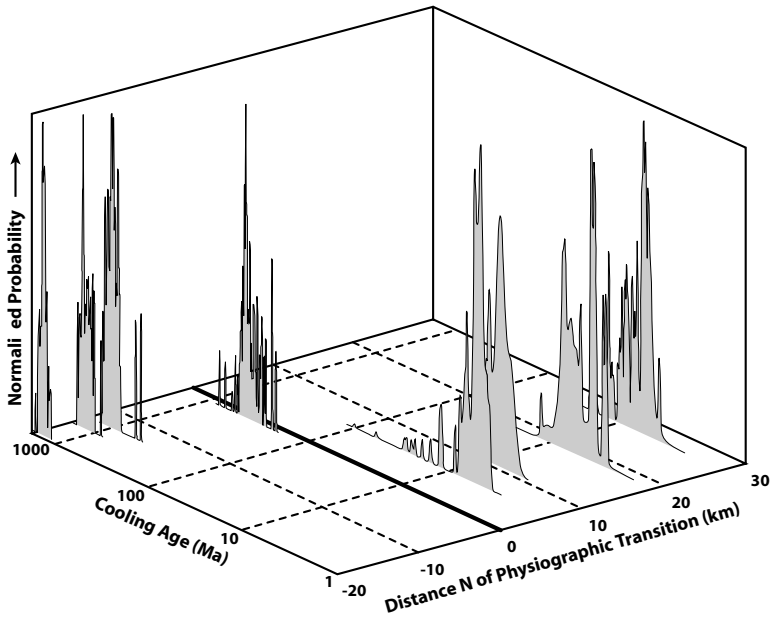

Figure 5. Stacked SPDF plots for $^{40}Ar/^{39}Ar$ muscovite dates from detrital samples from small catchments north and south of the physiographic transition separating the Higher and Lower Himalayan ranges in the Ganesh region of central Nepal, after Wobus et al. (2003). Note the logarithmic cooling age scale of the SPDF plots. The thick solid line at the physiographic transition marks a profound change in detrital cooling ages that is interpreted as a recently active, surface-breaking fault.

thermochronometers occur at mid-crustal levels, their use is particularly informative regarding long-term erosion rates in orogenic settings. Fission-track and (U-Th)/He thermochronometry of detrital accessory minerals, discussed elsewhere in this volume, provides similar information for regarding the cooling of source regions through lower-temperature, near-surface closure isotherms. The U-Pb zircon geochronometer has an extremely high closure temperature and is resistant to thermal resetting; thus, detrital zircon ages are seldom indicative of the thermal evolution of source regions during the most recent phase of mountain building (e.g., DeCelles et al. 2000). There have been some notable attempts to integrate some of these techniques to establish a better understanding of source regions and their thermal and erosional histories (e.g., Adams and Kelley 1998; Clift et al. 2004; Haines et al. 2004), but a systematic integration has yet to be done. A particularly high priority, for example, is the use of low-temperature thermochronometers to evaluate the tectonic significance of significant lag times documented by detrital mica $^{40}Ar/^{39}Ar$ thermochronometry for proximal deposits in the forelands of rapidly unroofed orogens like the Himalaya (White et al. 2002) .

Although the application of $^{40}Ar/^{39}Ar$ dating to ancient sediments has been highly successful, the method has only recently been used in the study of modern sediments. This is a particularly fruitful arena for research. For example, more aggressive dating campaigns in active foreland basins and river systems can help elucidate erosional patterns in developing orogens. Temporal variations in sediment storage in active river systems can be studied by applying the technique to fluvial terrace deposits, the ages of which might be determined by ^{14}C or cosmogenic dating methods. Moreover, the spatial patterns of glacial erosion can be addressed by detailed dating studies of moraine deposits.

As we learn more and more about the relationship between catchment-scale erosional processes and the apparent age distributions found in modern sediments, these lessons can be used to refine how we use data from more sedimentary rocks to study ancient landscapes. Stock and Montgomery (1996) anticipated such studies by suggesting how detrital thermochronologic data could be used to deduce paleorelief. While their method requires the assumption of a known geothermal gradient, a somewhat less dangerous assumption is that changes in geothermal gradient occur at slower rates than changes in relief, such that studies of changes in age ranges from one stratigraphic level to another can provide more reliable information about the evolution of relief in a sediment source region. Such unexploited opportunities ensure that detrital deposits will continue to be an attractive target for $^{40}Ar/^{39}Ar$ thermochronology.

REFERENCES

Aalto KR, Sharp WD, Renne PR (1998) $^{40}Ar/^{39}Ar$ dating of detrital micas from Oligocene-Pleistocene sandstones of the Olympic Peninsula, Klamath Mountains, and northern California Coast Ranges: provenance and paleodrainage patterns. Can J Earth Sci 35(7):735-745

Adams CJ, Kelley S (1998) Provenance of Permian-Triassic and Ordovician metagraywacke terranes in New Zealand; evidence from $^{40}Ar/^{39}Ar$ dating of detrital micas. Geol Soc Am Bull 110:422-432

Barbieri C, Carrapa B, Di Giulio A, Wijbrans J, Murrell GR (2003) Provenance of Oligocene synorogenic sediments of the Ligurian Alps (NW Italy): Inferences on belt age and cooling history. Int J Earth Sci 92: 758-778

Batt GE, Braun J (1997) On the thermomechanical evolution of compressional orogens. Geophys J Int 128: 364-382

Bernet M, Garver JI (2005) Fission-track analysis of detrital zircon. Rev Mineral Geochem 58:205-238

Bevington PR, Robinson DK (1992) Data Reduction and Error Analysis for the Physical Sciences. McGraw-Hill, Inc., New York

Brandon MT, Vance JA (1992) Fission-track ages of detrital zircon grains: Implications for the tectonic evolution of the Cenozoic Olympic subduction complex. Am J Sci 292:565-636

Braun J, Sambridge M (1997) Modelling landscape evolution on geological time scales: A new method based on irregular spatial discretization. Basin Res 9:27-52

Brewer ID (2001) Detrital-Mineral Thermochronology: Investigations of Orogenic Denudation in the Himalaya of Central Nepal, p. 181. The Pennsylvania State University, State College, PA.

Brewer ID, Burbank DW, Hodges KV (2003) Modelling detrital cooling-age populations: insights from two Himalayan catchments. Basin Res 15:305-320

Brewer ID, Burbank DW, Hodges KV (2005) Downstream development of a detrital cooling-age signal: insights from $^{40}Ar/^{39}Ar$ muscovite thermochronology in the Nepalese Himalaya. *In*: Tectonics, Climate, and Landscape Evolution. Geological Society of America Special Paper. Willett SD, Hovius N, Brandon MT, Fisher D (eds) Geological Society of America, Denver, in press

Carrapa B, Di Giulio A, Wijbrans J (2004a) The early stages of the Alpine collision: an image derived from the upper Eocene–lower Oligocene record in the Alps-Apennines junction area. Sed Geol 171:181-203

Carrapa B, Wijbrans J, Bertotti G (2003) Episodic exhumation in the Western Alps. Geology 31(7):601-604

Carrapa B, Wijbrans J, Bertotti G (2004b) Detecting differences in cooling/exhumation patterns within the Western Alpine arc through $^{40}Ar/^{39}Ar$ thermochronology on detrital minerals (Tertiary Piedmont Basin, NW Italy). *In:* Detrital Thermochronology – Provenance Analysis, Exhumation, and Landscape Evolution of Mountain Belts. Geological Society of America Special Paper 378. Bernet M, Spiegel C (eds.) Geological Society of America, Denver, p 67-103

Cerveny PF, Naeser ND, Zeitler PK, Naeser CW, Johnson NM (1988) History of uplift and relief of the Himalaya during the past 18 million years; evidence from sandstones of the Siwalik Group. *In:* New Perspectives in Basin Analysis. Kleinspehn KL, Paola C (eds) Springer-Verlag, New York, p 43-61

Cherniak DJ, Watson EB (2000) Pb diffusion in zircon. Chem Geol 172:5-24

Clift PD, Campbell IH, Pringle MS, Carter A, Zhang X, Hodges KV, Khan AA, Allen CM (2004) Thermochronology of the modern Indus River bedload: new insight into the controls on the marine stratigraphic record. Tectonics 23, doi:10.1029/2003TC001559

Copeland P, Harrison TM (1990) Episodic rapid uplift in the Himalaya revealed by $^{40}Ar/^{39}Ar$ analysis of detrital K-feldspar and muscovite, Bengal Fan. Geology 18:354-357

Dallmeyer RD, Keppie JD, Nance RD (1997) $^{40}Ar/^{39}Ar$ ages of detrital muscovite within Lower Cambrian and Carboniferous clastic sequences in northern Nova Scotia and southern New Brunswick; applications for provenance regions. Can J Earth Sci 34(2):156-168

Dallmeyer RD, Neubauer F (1994) Cadomian $^{40}Ar/^{39}Ar$ apparent age spectra of detrital muscovites from the Eastern Alps. J Geol Soc London 151:591-598

DeCelles PG, Gehrels GE, Quade J, LaReau B, Spurlin M (2000) Tectonic implications of U-Pb zircon ages of the Himalayan orogenic belt in Nepal. Science 288:497-499

Di Vincenzo G, Viti C, Rocchi S (2003) The effect of chlorite interlayering on 40Ar-39Ar biotite dating: an ^{40}Ar-^{39}Ar laser-probe and TEM investigations of variably chloritised biotites. Contrib Mineral Petrol 145: 643-658

Dong H, Peacor DR, Murphy SF (1998) TEM study of progressive alteration of igneous biotite to kaolinite throughout a weathered soild profile. Geochim Cosmochim Acta 62:1881-1887

Ehlers TA, Farley KA (2003) Apatite (U-Th)/He thermochronometry; methods and applications to problems in tectonic and surface processes. Earth Planet Sci Lett 206:1-14

Galbraith RF, Green PF (1990) Estimating the component ages in a finite mixture. Nucl Tracks Rad Meas 17: 197-206

Gehrels GE (2000) Introduction to detrital zircon studies of Paleozoic and Triassic strata in western Nevada and northern California. *In*: Paleozoic and Triassic Paleogeography and Tectonics of Western Nevada and Northern California. Geological Society of America Special Paper 347. Soreghan MJ, Gehrels GE (eds) Geological Society of America, Boulder, p 1-17

Gehrels GE, Stewart JH, Kettner KB (2002) Cordilleran-margin quartzites in Baja California – implications for tectonic transport. Earth Planet Sci Lett 199:201-210

Grimmer JC, Ratschbacher L, McWilliams M, Franz,L, Gaitzsch I, Tichomirowa M, Hacker BR, Yueqiao Z (2003) When did the ultrahigh-pressure rocks reach the surface? A $^{207}Pb/^{206}Pb$ zircon, $^{40}Ar/^{39}Ar$ white mica, Si-in-white mica, single-grain provenance study of Dabie Shan synorogenic foreland sediments. Chem Geol 197(1-4):87-110

Haines PW, Turner SP, Kelley SP, Wartho JA, Sherlock SC (2004) ^{40}Ar-^{39}Ar dating of detrital muscovite in provenance investigations: a case study from the Adelaide Rift Complex, South Australia. Earth Planet Sci Lett 227:297-311

Hames WE, Hodges KV (1993) Laser $^{40}Ar/^{39}Ar$ evaluation of slow cooling and episodic loss of ^{40}Ar from a sample of polymetamorphic muscovite. Science 261:1721-1723

Harrison TM, Copeland P, Hall SA, Quade J, Burner S, Ojha TP, Kidd WSF (1993) Isotopic preservation of Himalayan/Tibetan uplift, denudation, and climatic histories of two molasse deposits. J Geol 101:157-175

Harrison TM, Zeitler PK (2005) Fundamentals of noble gas thermochronometry. Rev Mineral Geochem 58: 123-149

Heller PL, Renne PR, O'Neil JR (1992) River mixing rate, residence time,, and subsidence rates from isotopic indicators: Eocene sandstones of the U.S. Pacific Northwest. Geology 20:1095-1098

Hemming SR, Bond GC, Broecker WS, Sharp WD, Klas-Mendelson M (2000) Evidence from $^{40}Ar/^{39}Ar$ ages of individual hornblende grains for varying Laurentide sources of iceberg discharges 22,000 to 10,500 yr B.P. Quaternary Res 54:372-383

Hemming SR, Hall CM, Biscaye PE, Higgins SM, Bond GC, McManus JF, Barber DC, Andrews JT, Broecker WS (2002) $^{40}Ar/^{39}Ar$ ages and $^{40}Ar^*$ concentrations of fine-grained sediment fractions from North Atlantic Heinrich layers. Chem Geol 182:583-603

Hodges K, Wobus C, Ruhl K, Schildgen T, Whipple K (2004) Quaternary deformation, river steepening, and heavy precipitation at the front of the Higher Himalayan ranges. Earth Planet Sci Lett 220:379-389

Hodges KV (1998) $^{40}Ar/^{39}Ar$ geochronology using the laser microprobe. *In*: Reviews in Economic Geology 7: Applications of Microanalytical Techniques to Understanding Mineralizing Processes. McKibben MA, Shanks WC (eds) Society of Economic Geologists, Tuscaloosa, p 53-72

Hodges KV (2003) Geochronology and Thermochronology in Orogenic Systems. *In*: The Crust, 3. Rudnick RL (ed) Elsevier Science, Amsterdam, p 263-292

Hodges KV, Bowring SA (1995) $^{40}Ar/^{39}Ar$ thermochronology of isotopically zoned micas; insights from the southwestern USA Proterozoic orogen. Geochim Cosmochim Acta 59(15):3205-3220

Huerta AD, Royden LH, Hodges KV (1998) The thermal structure of collisional orogens as a response to accretion, erosion, and radiogenic heating. J Geophys Res-Solid Earth103(B7):15287-15302

Hunecke JC, Smith SP (1976) The realities of recoil: ^{39}Ar recoil out of small grains and anomalous patterns in ^{40}Ar-^{39}Ar dating. Geochim Cosmochim Acta, Suppl 7:1987-2008

Hutson FE, Mann P, Renne PR (1998) $^{40}Ar/^{39}Ar$ dating of single muscovite grains in Jurassic siliciclastic rocks (San Cayetano Formation); constraints on the paleoposition of western Cuba. Geology 26(1):83-86

Kelley S (2002) Excess argon in K–Ar and Ar–Ar geochronology. Chem Geol:188:1-22

Kelley S, Bluck, BJ (1989) Detrital mineral ages from the Southern Uplands using ^{40}Ar-^{39}Ar laser probe. J Geol Soc London146(3):401-403

Kelley SP, Bluck BJ (1992) Laser ^{40}Ar-^{39}Ar ages for individual detrital muscovites in the Southern Uplands of Scotland, U.K. Chem Geol 101(1-2):143-156

Kowalewski M, Rimstidt JD (2003) Average lifetime and age spectra of detrital grains: Toward a unifying theory of sedimentary particles. J Geology 111:427-439

Lague D, Crave A, Davy P (2003) Laboratory experiments simulating the geomorphic response to tectonic uplift. J Geophys Res 108, doi:10.1029/2002JB001785

Lin L-H, Onstott TC, Dong H (2000) Backscattered ^{39}Ar loss in fine-grained minerals: implications for $^{40}Ar/^{39}Ar$ geochronology of clay. Geochim Cosmochim Acta 64:3965-3974

Lovera OM, Grove M, Harrison TM (2002) Systematic analysis of K-feldspar Ar-40/Ar-39 step heating results II: relevance of laboratory argon diffusion properties to nature. Geochim Cosmochim Acta 66(7):1237-1255

Mancktelow NS, Grasemann B (1997) Time-dependent effects of heat advection and topography on cooling histories during erosion. Tectonophysics 270:167-195

Markley MJ, Teyssier C, Cosca M (2002) The relation between grain size and $^{40}Ar/^{39}Ar$ date for Alpine white mica from the Siviez-Mischabel Nappe, Switzerland. J Struct Geol 24(12):1937-1955

McDougall I, Harrison TM (1998) Geochronology and Thermochronology by the $^{40}Ar/^{39}Ar$ Method. Oxford University Press, New York

Mitchell JG, Penven MJ, Ineson PR, Miller JA (1988) Radiogenic argon and major-element loss from biotite during natural weathering – a geochemical approach to the interpretation of potassium-argon ages of detrital biotite. Chem Geol 72:111-126

Murphy SF, Brantley SL, Blum AE, White AF, Dong H (1998) Chemical weathering in a tropical watershed, Luquillo Mountains, Puerto Rico: II. Rate and mechanism of biotite weathering. Geochim Cosmochim Acta 62:227-243

Najman Y, Garzanti E, Pringle M, Bickle M, Stix J, Khan I (2003) Early-middle Miocene paleodrainage and tectonics in the Pakistan Himalaya. Geol Soc Am Bull 115(10):1265-1277

Najman Y, Pringle M, Godin L, Oliver G (2001) Dating of the oldest continental sediments from the Himalayan foreland basin. Nature 410(6825):194-197

Najman Y, Pringle M, Godin L, Oliver G (2002) A reinterpretation of the Balakot Formation: Implications for the tectonics of the NW Himalaya, Pakistan. Tectonics 21(5), doi:10.1029/2001TC001337

Najman YMR, Pringle MS, Johnson MRW, Robertson AHF, Wijbrans JR (1997) Laser Ar-40/Ar-39 dating of single detrital muscovite grains from early foreland-basin sedimentary deposits in India: Implications for early Himalayan evolution. Geology 25(6):535-538

Onstott TC, Miller ML, Ewing RC, Arnold GW, Walsh DS (1995) Recoil refinements: Implications for the $^{40}Ar/^{39}Ar$ dating technique. Geochim Cosmochim Acta 59:1821-1834

Parsons I, Brown WL, Smith JV (1999) $^{40}Ar/^{39}Ar$ thermochronology using alkali feldspars: real thermal history or mathematical mirage of microtexture? Contrib Mineral Petrol 136:92-110

Rahman MJJ, Faupl P (2003) $^{40}Ar/^{39}Ar$ multigrain dating of detrital white mica of sandstones of the Surma Group in the Sylhet Trough, Bengal Basin, Bangladesh. Sed Geol 155(3-4):383-392

Renne PR, Becker TA, Swapp SM (1990) $^{40}Ar/^{39}Ar$ laser-probe dating of detrital micas from the Montgomery Creek Formation, Northern California; clues to provenance, tectonics, and weathering processes. Geology 18(6):563-566

Renne PR, Swisher CC, Deino AL, Karner DB, Owens T, DePaolo DJ (1998) Intercalibration of standards, absolute ages and uncertainties in $^{40}Ar/^{39}Ar$ dating. Chem Geol (Isotope Geosciences) 145:117-152

Roberts HJ, Kelley SP, Dahl PS (2001) Obtaining geologically meaningful ^{40}Ar-^{39}Ar ages from altered biotite. Chem Geol 172(3-4):277-290

Ross GM, Bowring SA (1990) Detrital zircon geochronology of the Windermere Supergroup and the tectonic assembly of the southern Canadian Cordillera. J Geol 98:879-893

Ruhl KW, Hodges KV (2005) The use of detrital mineral cooling ages to evaluate steady-state assumptions in active orogens: an example from the central Nepalese Himalaya. Tectonics, in press

Ruiz GMH, Seward D, Winkler W (2004) Detrital thermochronology – a new perspective on hinterland tectonics, an example from the Andean Amazon Basin, Ecuador. Basin Res 16, doi:10.1111/j.1365-2117.2004.00239.x

Safran EB (2003) Geomorphic interpretation of low-temperature thermochronologic data: Insights from two-dimensional thermal modeling. J Geophys Res 108, doi:10.1029/2002JB001870

Sambridge MS, Compston W (1994) Mixture modeling of multicomponent data sets with application to ion probe zircon ages. Earth Planet Sci Lett 128: 373-390

Scaillet S (1996) Excess ^{40}Ar transport scale and mechanism in high-pressure phengites; a case study from an eclogitized metabasite of the Dora-Maira nappe, Western Alps. Geochim Cosmochim Acta 60:1075-1090

Sherlock SC (2001) Two-stage erosion and deposition in a continental margin setting; an $^{40}Ar/^{39}Ar$ laserprobe study of offshore detrital white micas in the Norwegian Sea. J Geol Soc London 158(5):793-799

Sherlock SC, Jones KA, Kelley SP (2002) Fingerprinting polyorogenic detritus using the $^{40}Ar/^{39}Ar$ ultraviolet laser microprobe. Geology 30(6):515-518

Sircombe KN (2004) AGEDISPLAY: an EXCEL workbook to evaluate and display univariate geochronological data using binned frequency histograms and probability density distributions. Computers & Geosciences 30(1):21-31

Sircombe KN, Hazelton ML (2004) Comparison of detrital zircon age distributions by kernel function estimation. Sed Geol 171:91-111

Stock JD, Montgomery DR (1996) Estimating paleorelief from detrital mineral age ranges. Basin Res 8:317-327

Stuart FM (2002) The exhumation history of orogenic belts from $^{40}Ar/^{39}Ar$ ages of detrital micas. Mineral Mag 66:121-135

Stuart FM, Bluck BJ, Pringle MS (2001) Detrital muscovite $^{40}Ar/^{39}Ar$ ages from Carboniferous sandstones of the British Isles: Provenance and implications for the uplift history of orogenic belts. Tectonics 20(2): 255-267

Stüwe K, Hintermüller M (2000) Topography and isotherms revisited: the influence of laterally migrating drainage divides. Earth Planet Sci Lett 184:287-303

Stüwe K, White L, Brown R (1994) The influence of eroding topography on steady-state isotherms. Application to fission track analysis. Earth Planet Sci Lett 124:63-74

Vermeesch P (2004) How many grains are needed for a provenance study? Earth Planet Sci Lett 224:441-451

von Eynatten H, Gaup R, Wijbrans JR (1996) $^{40}Ar/^{39}Ar$ laser-probe dating of detrital white micas from Cretaceous sedimentary rocks of Eastern Alps: evidence for Variscan high-pressure metamorphism and implications for Alpine Orogeny. Geology 24:691-694

von Eynatten H, Wijbrans J (2003) Precise tracing of exhumation and provenance using $^{40}Ar/^{39}Ar$ geochronology of detrital white mica: the example of the Central Alps. *In*: Tracing Tectonic Deformation Using the Sediment Record. Geological Society Special Publication 208. McCann T, Saintot A (eds) The Geological Society, London, p 289-305

Wagner GA, Reimer GM (1972) Fission track tectonics: The tectonic interpretation of fission track apatite ages. Earth Planet Sci Lett 14:263-268

Whipple KX (2001) Fluvial landscape response time: How plausible is steady-state denudation? Am J Sci 301: 313-325

White NM, Pringle M, Garzanti E, Bickle M, Najman Y, Chapman H, Friend P (2002) Constraints on the exhumation and erosion of the High Himalayan Slab, NW India, from foreland basin deposits. Earth Planet Sci Lett 195(1-2):29-44

Willett SD, Brandon MT (2002) On steady states in mountain belts. Geology 30:175-178

Wobus C, Heimsath A, Whipple K, Hodges K (2005) Active surface thrust faulting in the central Nepalese Himalaya. Nature 434:1008-1010

Wobus CW, Hodges KV, Whipple KX (2003) Has focused denudation sustained active thrusting at the Himalayan topographic front? Geology 31:861-864

Zeitler PK, Meltzer AS, Koons PO, Craw D, Hallet B, Chamberlain CP, Kidd WSF, Park SK, Seeber L, Bishop M, Shroder J (2001) Erosion, Himalayan geodynamics, and the geomorphology of metamorphism. GSA Today 11:4-9